SCIEPublish

Article

Calcite as a Mineralizer and Stabilizer for Low-Cost Zirconia-Mullite-Alumina Composites Synthesized from Siliceous Clay, Alumina and Zirconia

Somnath Mandal [1,*,†], Harshit Agrawal [1,‡], Abhijeet Phatak [1], Prashant Gupta [1,§], Ilona Jastrzębska [2], Om Parkash [1] and Devendra Kumar [1]

[1] Department of Ceramic Engineering, Indian Institute of Technology (Banaras Hindu University), Varanasi 221005, Uttar Pradesh, India; harshit.agrawal@iiml.org (H.A.); abhijeet.prajendra.cer11@iitbhu.ac.in (A.P.); prashant.gupta@wustl.edu (P.G.); oprakash.cer@iitbhu.ac.in (O.P.); devendra.cer@iitbhu.ac.in (D.K.)

[2] Faculty of Materials Science and Ceramics, AGH University, al. Mickiewicza 30, 30-059 Kraków, Poland; ijastrz@agh.edu.pl (I.J.)

* Corresponding author. E-mail: somnath.mandal@vesuvius.com (S.M.)

† Present address: Steel Flow Control Group, Vesuvius Research, Pittsburgh, PA 15205, USA.

‡ Present address: Cost and Productivity Reinvention, Accenture Strategy & Consulting, Gurugram 122002, India.

§ Present address: Department of Anesthesiology and Washington University Pain Center, Washington University School of Medicine, St. Louis, MO 63110, USA.

Received: 30 September 2024; Accepted: 14 November 2024; Available online: 19 November 2024

ABSTRACT: Fused zirconia-mullite (ZM) and zirconia-alumina (ZA) are expensive aggregates used in refractory formulations to enhance thermal shock tolerance and corrosion resistance, respectively. A cost-effective alternative approach was explored in this work to produce 37.4 wt% ZrO_2 containing ZM utilizing conventional reaction sintering of siliceous clay, calcined alumina and monoclinic ZrO_2. A series of chemical reactions ensued from 1200 °C, forming low quartz and cristobalite from the clay, in situ $ZrSiO_4$, monoclinic ZrO_2, α-Al_2O_3 and traces of leucite. 1600 °C was required to fully form mullite and monoclinic ZrO_2 but it had 26.5% porosity even after firing at 1650 °C for 2 h. It consisted of small equiaxed primary mullite grains secondary mullite rods, and scattered and clustered, round ZrO_2 grains. With 1.05% CaO addition, tetragonal ZrO_2 formed, but 22.7% porosity remained despite the presence of 13.5% liquid phase having a low viscosity (0.6 Pa.s, from FactSage). With 2.11% CaO, porosity reduced to 10.7% but mullite partly dissolved, forming α-Al_2O_3 (ZMA aggregate). The added CaO mostly remained in the intergranular glassy phase rather than inside the ZrO_2 grains but increased the thickness of the secondary mullite and the ZrO_2 grains. Mullite was completely lost with 4.21% CaO doping but favorably formed cubic ZrO_2 containing up to 0.26 at% Ca, interlinked α-Al_2O_3 rods and attained a low porosity of 0.2%. This ZA aggregate is limited to 1550 °C application temperature as excess liquid phase drained out beyond that. 7.37% CaO addition was detrimental as it formed an excessive anorthite-like liquid phase that percolated out at 1550 °C with 5.6% weight loss. Thus, in ZM-based calcium aluminate cement bonded refractory castables, the final CaO content should be restricted to below 2.1% to avoid partial dissolution of mullite.

Keywords: Alumina; Ceramic composites; Clay; Mullite; Refractory; Zirconia

1. Introduction

Zirconia-mullite (ZrO_2-$3Al_2O_3.SiO_2$, ZM) has diverse applications in engineering ceramics and refractories [1,2]. Mullite, having a very low thermal expansion coefficient (~5.5×10^{-6} K^{-1} at 25–1000 °C) [1] and high creep resistance, forms a strong matrix and often possesses a microstructure consisting of interlocked elongated or columnar grains. The zirconia phase has a high corrosion resistance, hardness and abrasion resistance [2]. Moreover, the presence of zirconia in ZM composites increases its fracture toughness [3] and enhances thermal shock resistance [4] due to microcrack toughening [5], which may be caused by the tetragonal to monoclinic polymorphic transformation-induced volume changes [1]. As a result, ZM composites exhibit a unique combination of superior tolerance to wear, thermal shock and

https://doi.org/10.70322/htm.2024.10009

high fracture toughness, along with good corrosion resistance [1]. Thus, sintered ZM is used to make wear- resistant components and analytical lab-wares [6]. Fused ZM aggregates are used to make ceramic pressure casting tubes, slide gate refractory (SGR) plates [7], submerged entry nozzles (SEN) and monoblock stoppers for continuous casting of steel [8], furnace charging holes, foundry coatings, ceramic rollers [9] and monolithic refractories used in the backup lining of the floor and side wall of glass melting furnaces [10–12]. Large fused ZrO_2-Al_2O_3-SiO_2 blocks with 33–40 wt% ZrO_2 are utilized as the hot face of glass melting tank furnaces [13,14].

Fused ZM aggregates that are used as raw materials for refractories applied in the glass and steel industries typically have 36–39 wt% ZrO_2 (with some HfO_2), 44–45.8% Al_2O_3, 17.5–18% SiO_2, 0.5–0.9% impurities (Na_2O, K_2O, Fe_2O_3, TiO_2, CaO, MgO), 2.5–3% open porosity, 3.58–3.66 g/cm^3 bulk density [8,11,15] and are estimated to be composed of 59 wt% mullite, 36% monoclinic ZrO_2 and 5% glass. They are obtained by the electric arc furnace (EAF) fusion of zircon ($ZrSiO_4$) sand and Bayer process alumina, and the microstructure consists of large needle-shaped mullite (100 µm thick), precipitated round and sometimes dendritic monoclinic zirconia, along with glass typically located adjacent to the mullite phase [11]. ZM is a relatively expensive ingredient in a refractory formulation compared to alumina, mullite and magnesia. However, it imparts corrosion resistance in the case of glass melting applications and provides high thermal shock resistance to steelmaking refractories due to its low and unique thermal expansion pattern caused by the monoclinic zirconia's phase transformation that hinders crack propagation by microcrack toughening [7,8]. Fused calcia stabilized zirconia having 95% ZrO_2+HfO_2, 4% CaO, 0.8% impurities (SiO_2, Al_2O_3, TiO_2, Fe_2O_3, MgO), 68–85% cubic zirconia phase, 15–32% monoclinic zirconia, 5.8 g/cm^3 density is an even more expensive refractory raw material used for its high corrosion resistance in SEN, tundish nozzles, SGR plates, kiln furniture for electro-ceramics and coating for investment casting molds [16,17]. Fused zirconia-alumina (ZA) with 25–43 wt% ZrO_2 is another strategic raw material used in SGR to improve its thermal shock tolerance and corrosion resistance [7,18].

Apart from the commercial EAF process, dense ZM had been experimentally prepared from plasma arc fusion of natural sillimanite, zircon sand and refractory-grade calcined alumina [6], transferred arc plasma melting of zircon and bauxite [19], and thermal plasma fusion of zircon and alumina [20]. The phase evolution during the solidification of Al_2O_3-ZrO_2-SiO_2 melt and subsequent reheating was also deeply investigated [21]. Additionally, zircon-alumina mixtures had been plasma sprayed into powders and subsequently spark plasma sintered to prepare ZM composites [22]. Moreover, microwave sintering at 1500 °C for 1h had been successfully used to achieve 92% density in mullite-20 wt% ZrO_2-1% MgO composition [23]. 0.2 µm mullite powder containing 5–80 vol% of 0.3 µm 3 mol% Y_2O_3 stabilized ZrO_2 had been hot-pressed at 1600 °C for 45 min to 95–98% density [24]. Unfortunately, these advanced manufacturing technologies are cost-prohibitive for producing refractory raw materials.

Pure mullite is difficult to fully sinter below 1700 °C [25] as even <1 µm preformed mullite powder could only attain 84% density after conventional sintering at 1610 °C for 6 h [5]. Hence, to prepare refractory-grade ZM without commercial EAF fusion or expensive advanced ceramic processing techniques, using only conventional sintering, one can: (i) reduce the starting particle size while being careful that below a d_{50} of 3–5 µm milling becomes costly, (ii) use sintering aids without deteriorating thermomechanical and corrosion properties, and (iii) fire in two stages [26] to separate reaction accompanied by volume expansion from densification. The use of natural raw materials [27,28] in whole or in part can be a smart choice as the impurities can provide the required liquid phase sintering aids, as long as they are not too high so as to deteriorate the aggregate/matrix bonding and thereby hot strength [29]. Very fine, thermochemically treated clay-derived mullite precursor [3] with 250 m^2/g surface area (for reference, common refractory grade calcined alumina with a d_{50} of 8.9 µm has 0.9 m^2/g) [30] combined with up to 20 vol% ZrO_2 were densified at 1570 °C for 2.5 h and attained higher density (99%) than pure mullite (97%) [3]. Dense ZM had been reaction sintered at 1600 °C for 4 h when 1 µm zircon and 0.5 µm α-Al_2O_3 were used [4] or within 1520 °C when mixtures of 0.2 µm zirconia and 1.5 µm mullite, 0.7 µm zircon and 0.4 µm alumina, as well as zirconia, alumina and 12 nm fumed silica were used [31]. Zircon and alumina ball milled to a d_{50} of 0.3 µm is known to achieve higher density (94%) after firing at 1600 °C for 2 h than mixtures of zircon and $Al(OH)_3$ calcined and ground to a d_{50} of 3.8 µm, as well as zircon and $Al(NO_3)_3$ heated and milled to 11.5 µm [32]. Unfortunately, many of the aforementioned powder sizes can be too expensive for a refractory.

Due to the difficulty in sintering ZM of commonly available particle sizes (e.g., <75 µm), several additives had been explored to reduce the temperature for phase formation and densification. TiO_2, when added to zircon-alumina mixture formed zirconia and mullite at a lower temperature, increased bulk density [33], reduced apparent porosity [34], and attained higher tetragonal zirconia phase content at 1400 °C [33]. For 7.5–10 wt% rutile TiO_2 doping, tialite (Al_2TiO_5) formed, but hot modulus of rupture (HMOR) and soda-lime-silica melt corrosion resistance were only better for the 2.5% TiO_2 doped ZM and reduced beyond that [34].

Oxides of rare earth elements (REEO) also proved to be effective dopants for ZM. Adding 1–3 mol% Y_2O_3 to sol-gel derived mullite containing 15–20 vol% ZrO_2 partially stabilized the ZrO_2 in the tetragonal phase (6–34%) attaining full density [25]. 2–3 mol% Y_2O_3 had been used to assist densification of sub-micron preformed mullite [5]. In ZM prepared from sillimanite-alumina-zirconia mixtures, Y_2O_3 addition had steadily increased the tetragonal zirconia content, but 4–8 mol% Y_2O_3 addition worsened apparent porosity at 1550–1600 °C and only the 2 mol% Y_2O_3 added ZM had higher HMOR [35]. Up to 7 mol% (4.1 wt%) Y_2O_3 addition to 2:3 molar zircon: alumina mixture (which would have formed one mole each of zirconia and mullite) improved densification at 1500 °C increased the tetragonal zirconia phase at 1550 °C (22.2% in undoped *vs.* 65.8%) as well as the flexural strength (154 *vs.* 256 MPa), and reduced the thermal expansion coefficient [36]. CeO_2 is also an effective REEO sintering aid for ZM [37]. CeO_2 addition to zircon-alumina mixture retards zircon dissociation and benefits by direct conversion into zirconia and mullite along with the formation of cerium aluminosilicate liquid phase and CeO_2-ZrO_2 solid solution resulting in a higher yield of mullite and tetragonal zirconia [38]. 2.5–4.5 mol% Dy_2O_3 addition to zircon-alumina mixture improved its densification by forming a liquid phase, increased tetragonal zirconia content from 11 (in undoped ZM) to ~26%, went into solid solution with both zirconia and mullite and reduced the thermal expansion coefficient from 4.9 to 3.5 × 10^{-6} K^{-1} (25–1400 °C) [39].

Using a liquid phase forming additive like 1.8 wt% MgO had successfully sintered ZM at 1500 °C [26]. However, 2.1 wt% MgO addition to ZM derived from sillimanite, alumina and zirconia was reported to reduce HMOR at 1250 °C [40]. During reaction sintering of zircon-alumina 20:80 wt% mixture, it had been observed that at 1550 °C for 5h, 10 wt% MgO addition caused corundum to be reduced from 64 to 57%, mullite increased from 20 to 25%, monoclinic zirconia reduced from 12 to 9% and no $MgAl_2O_4$ spinel remained [41]. CaO is also an effective sintering aid for ZM [37]. For a 4.7 wt% CaO doped ZM with 41.2% ZrO_2, it had been clarified that a transitory liquid phase appears at 1200 °C, but at 1450 °C, anorthite disappears, zircon dissociates appreciably, a permanent liquid forms and rapid sintering shrinkage occurs providing double the fracture toughness than pure mullite (4.3 *vs.* 2.0 MPa√m) [42]. Compared to MgO, whereas CaO attained higher densification, but 10 wt% CaO addition produced 64% corundum, unfortunately no mullite, 7% monoclinic zirconia, 9% hibonite ($CaO.6Al_2O_3$), 7% $CaZrO_3$ and 1% anorthite ($CaAl_2Si_2O_8$ or $CaO.Al_2O_3.2SiO_2$) [41].

Obtaining dense ZM aggregates by sintering below 1550 °C is possible using submicron powders, but such fine powders are costly and limited to application in engineering ceramics. High-volume consumers like the refractory industry need coarser, lower-price ingredients. Inspired by the expensive commercial fused ZM and CaO stabilized zirconia refractory raw materials, this study uniquely utilizes cost-effective, common Indian siliceous clay and commercial calcined alumina as mullite precursors. The high silica in the clay obviated the need for zircon,so monoclinic zirconia was used instead. The evolution of the phases was studied from 1200 °C to 1600 °C to reveal the reactions between the raw materials and to identify the temperature at which zirconia and mullite fully develop. The impact of the addition of ubiquitously available calcite ($CaCO_3$) was studied, which provided CaO aimed to accelerate densification by generating a eutectic calcium aluminum silicate glassy phase and perhaps partially stabilize the zirconia [26,42,43]. The densification, phase and microstructure development were critically discussed and correlated with FactSage thermodynamic calculations. This research is intended to be useful for forming in situ ZM in a refractory brick matrix, understanding fused ZM-lime reactions in calcium aluminate cement bonded refractory castables [12] and developing wear-resistant ceramic tiles [6].

2. Materials and Methods

Low-cost, siliceous clay was sourced from Jharkhand, India. The raw clay had a weight loss on ignition (LOI) of 7.95%, which indicated that it was low in kaolinite ($Al_2O_3.2SiO_2.2H_2O$) as kaolinitic clays, often called flint clays by refractory makers, have an LOI of 13–15% when they don't have much organics [44,45]. The composition of the calcined clay measured by X-ray fluorescence (XRF, Optim'X, Thermo ARL, Switzerland) was 61.66 wt% SiO_2, 27.59% Al_2O_3, 0.90% Fe_2O_3, 0.89% TiO_2, 0.10% Na_2O and 0.91% K_2O. This clay was silica-rich and alumina-deficient compared to flint clays that typically have 50–56% SiO_2 and 42–45% Al_2O_3 after calcination [44–46]. Powder X-ray diffraction (XRD, Miniflex II, Desktop X-ray diffractometer, Rigaku corporation, Tokyo, Japan) was done in the range 10–80° 2θ with a 0.02° step size. At first, the raw XRD intensity of each sample was converted into relative intensity (%) followed by plotting in OriginPro 2022b software. Then each peak was manually listed in a Microsoft Excel spreadsheet and matched with fixed slit intensity tables in International Center for Diffraction Data Powder Diffraction Files (ICDD PDF) [47]. Low quartz or α-quartz (ICDD 00-046-1045, hexagonal crystal structure, space group P3221) was the major phase in the siliceous clay (Figure 1a), closely matching with the 100% intensity peak (26.62° *vs.* 26.639°).

The 15% intensity peak of the clay coincided with kaolinite (ICDD 00-089-6538, end-centered triclinic structure, space group C1) with excellent 2θ match (12.36° *vs.* 12.355°). Another kaolinite type, 1AA (ICDD 01-078-2110, triclinic structure, space group P1) was needed to index the remaining peaks, although it had slight shifts (e.g., 20.46° *vs.* 20.377°). It should be noted that all peaks of the first kaolinite overlapped with kaolinite-1AA, but the first one was closer to the experimental 2θ, while the second one helped in matching few extra peaks. Three peaks at 21.78°, 25.28° and 27.94° with up to 5.4% background subtracted intensity remained unidentified. Simultaneous differential thermal analysis and thermo-gravimetry (DTA-TG) of the as-received clay (89 mg sample) were done in a Netzsch instrument in simulated air atmosphere (N_2:O_2 4:1 flow rate) at a ramp of 10 K/min up to 1350 °C. At 105 °C (Figure 1b), a broad endothermic peak concomitant with a small weight loss (0.1%) was seen due to the loss of free water (moisture). A tiny endothermic peak at 418 °C was seen with an associated change in slope of the TG curve and 0.9 wt% loss. This may be due to the burning of organic matter in the clay as this has been reported to occur at 447 °C which was corroborated by CO_2 detection [44]. At 528 °C (Figure 1b), a major endothermic peak with simultaneous large weight loss was observed because of the de-hydroxylation of kaolinite resulting in the formation of amorphous metakaolinite ($Al_2O_3.2SiO_2$), in line with literature reporting this at 507–516 °C [44]. The weight loss continued to about 700 °C after which it stabilized at 6.1%. Later, a sharp exothermic peak occurred at 995 °C without any weight loss and is ascribed to the formation of mullite crystals typically reported for kaolinitic clays at 986–989 °C [44].

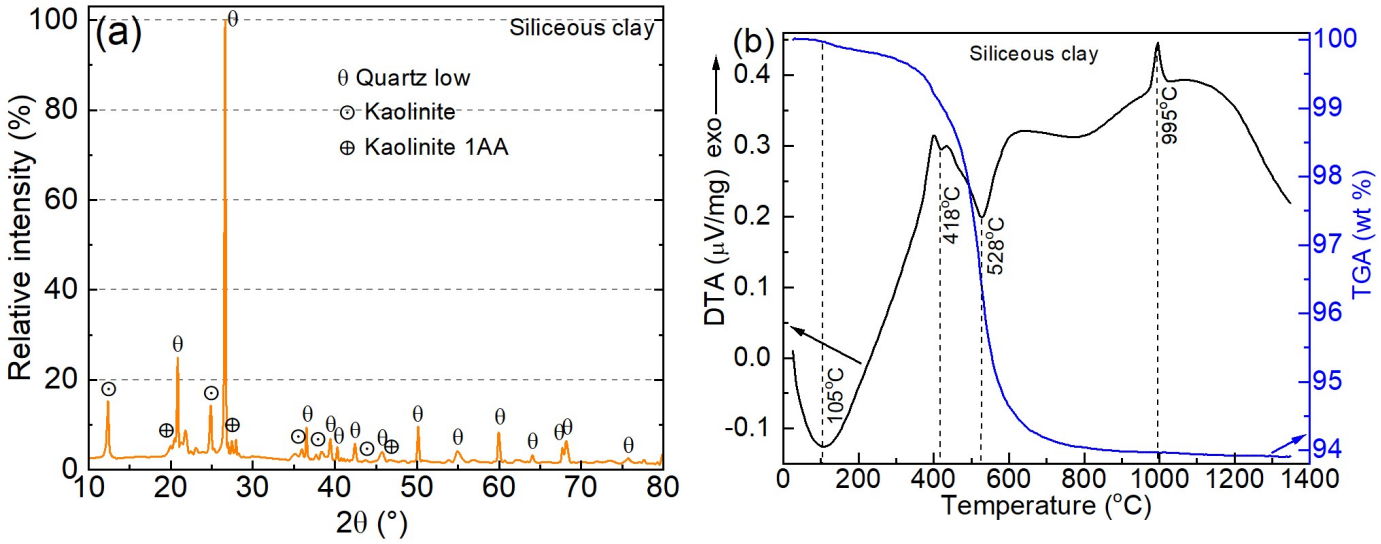

Figure 1. (**a**) Powder XRD pattern and (**b**) DTA-TG curves of the siliceous clay.

To fully convert the siliceous clay into mullite, the required amount of refractory-grade calcined alumina (99.6% pure, described in [48]) was used. XRD (Figure 2a) showed it contained mainly corundum (α-Al_2O_3, ICDD 00-046-1212, rhombohedral structure, space group R-3C) with a close match for the tallest peak (35.12° *vs.* 35.152°). A small amount of β-Al_2O_3 or diaoyudaoite ($Na_2O.11Al_2O_3$, ICDD 04-010-0578, hexagonal structure, P63/mmc space group) was found matching with the 8.4% intensity peak (15.66° *vs.* 15.723°) arising due to ~0.3% Na_2O (+K_2O) [48] from the Bayer process. The ZrO_2 source in ZM was lab-grade zirconia (Loba Chemie, Mumbai, India) with 99.5% ZrO_2, 0.12% SiO_2, 0.007% TiO_2, 0.002% Fe_2O_3, 5.7 g/cm^3 pycnometric density and 11–39 μm particle size (d_{10}–d_{90}). Figure 2b shows monoclinic ZrO_2 (ICDD 00-037-1484, space group P21/a) was its major phase (28.24° *vs.* 28.175° for the tallest peak) along with a small amount of tetragonal ZrO_2 (ICDD 00-050-1089, space group P42/nmc) matching the 18.9% intensity peak with good 2θ match (30.32° *vs.* 30.27°). Two peaks at 25.50° and 58.02° with 1.2% and 4.2% background subtracted intensity remained unidentified. The CaO mineralizer's source was lab-grade calcite or calcium carbonate (Thomas Baker, Mumbai, India) of 99.5% purity with 0.03% Na, 0.005% K, 0.02% Mg, 0.001% Fe, 0.03% Ba, 0.10% NH_4^+, 0.005% Cl^-, 0.01% NO_3^- and LOI of 44.0%.

Siliceous clay lumps were crushed in an agate mortar and pestle, calcined at 700 °C for 2 h for de-hydroxylation of kaolinite (Figure 1b) and sieved to obtain <75 μm. Calcined clay, alumina and zirconia were weighed per composition C0 shown in Table 1, such that the final reaction sintered product would have an estimated composition as provided in Table 2, which would mimic the chemistry of commercial fused ZM refractory aggregates [8,11]. To the base ZM composition, C0, the calculated amounts of $CaCO_3$ (considering its LOI) were added to synthesize C1, C2, C4 and C7 with 1.05, 2.11, 4.21 and 7.37 wt% CaO, respectively. A 3.85 wt% concentration aqueous solution of polyvinyl alcohol

(PVA, Loba Chemie, India) was made on a hot plate with a magnetic stirrer at 84–96 °C for 2 h. 30 g batches were weighed and mixed in a mortar and pestle, then 5% (1.5 g) of the PVA binder solution was added. This was mixed and screened five times through a 500 µm sieve for granulation. The moist powder granules were then uniaxially pressed into pellets of diameter 15 mm and thickness 8 mm by dwelling at 44 MPa for 10 s (de-airing) and then at 152 MPa for 1 min. The pellets were then dried overnight in an oven at 120 °C. Finally, they were fired in an electrically heated alumina tube furnace (Electroheat, Naskar and Co., Howrah, India) in air at 5 K/min with a 2 h soaking at the maximum temperature followed by controlled cooling at 5 K/ min to 800 °C and natural cooling after that.

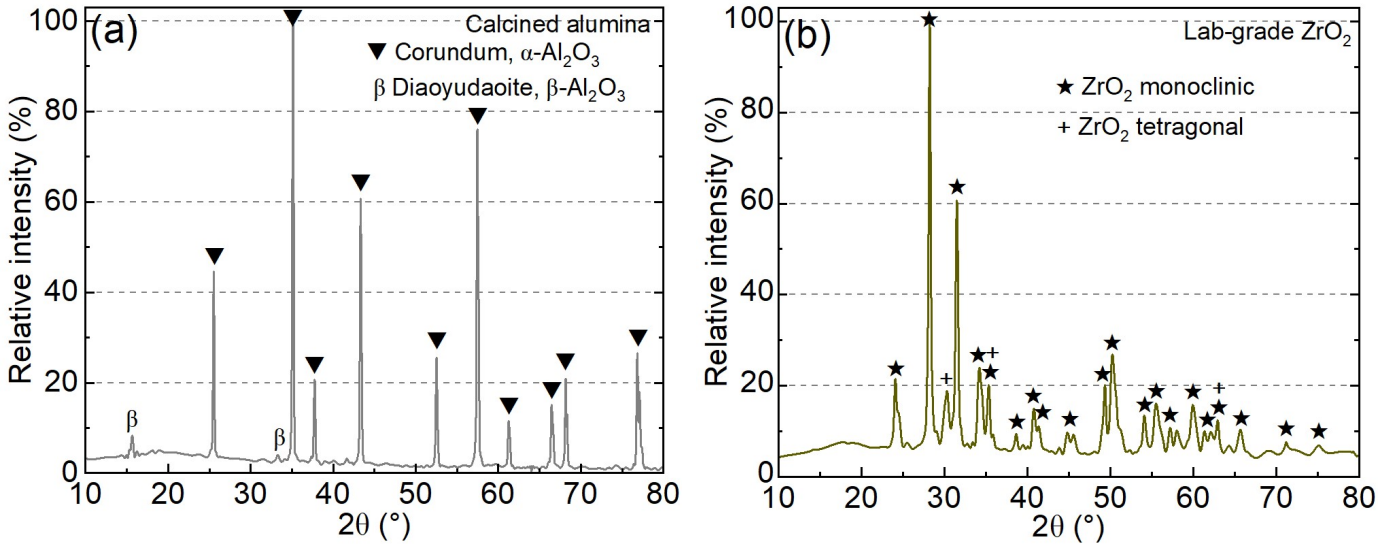

Figure 2. XRD pattern of raw materials (**a**) industrial calcined alumina and (**b**) lab-grade zirconia.

Table 1. Batch composition (wt%).

Composition	Zirconia	Calcined Clay	Alumina	Calcite
C0	37.50	26.00	36.50	0.00
C1	36.84	25.54	35.85	1.77
C2	36.18	25.10	35.20	3.52
C4	34.90	24.24	33.94	6.92
C7	33.18	22.74	32.22	11.86

Table 2. Expected composition (wt%) after sintering.

Composition	Al_2O_3	SiO_2	ZrO_2	Fe_2O_3	TiO_2	Na_2O	K_2O	CaO
C0	44.24	17.45	37.39	0.25	0.25	0.14	0.26	0.00
C1	43.78	17.27	37.01	0.25	0.25	0.14	0.25	1.05
C2	43.30	17.10	36.61	0.25	0.25	0.14	0.25	2.11
C4	42.36	16.75	35.82	0.24	0.24	0.13	0.25	4.21
C7	40.98	16.04	34.77	0.23	0.23	0.13	0.24	7.37

Densification of the fired composites was studied by measuring bulk density and apparent porosity using the Archimedes technique in boiling water for 2 h, similar to ASTM C20-00 standard [49]. Phase evolution of sintered samples was investigated by powder XRD, which was also supported by thermodynamic equilibrium calculations using FactSage software version 7.3 using its Equilib module and FactPS, FToxid and FTmisc databases. Some fired samples were ground and polished using different sizes of SiC powder with water on a rotating disc. Also, fracture surfaces of sintered samples were prepared for microstructural observation. After sputter coating with gold (Hummer sputtering system, LADD Research, USA), images were taken using a scanning electron microscope (SEM, Inspect S50, FEI, Magnetgatan, Sweden) operated at 12.5–17 kV. Chemical microanalysis was performed on polished surfaces using another SEM (Carl Zeiss Microscopy, EVO MA 15/18) that was equipped with an energy dispersive spectrometer (EDS, 51N1000, Oxford Instruments, UK) operated at 20 kV. Average grain size was measured on 7–39 grains of each phase per sample using Image J software (version 1.53e, National Institute of Health, Bethesda, MD, USA).

3. Results and Discussion

3.1. Phase Evolution of Undoped ZM Formulations

The major phase in C0, the undoped formulation that mimics commercial fused ZM, after firing at 1200 °C (Figure 3a), was monoclinic ZrO_2 with a close match (e.g., 28.20° *vs.* 28.175°). A large amount of unreacted α-Al_2O_3 remained, matching with the 62.0% intensity peak (35.16° *vs.* 35.152°). Several peaks of low quartz from clay remained with up to 43.0% intensity with a good match (26.60° *vs.* 26.639°). Cristobalite SiO_2 (ICDD 00-039-1425, tetragonal structure, space group P41212) with up to 13.1% intensity remained, which probably crystallized from the amorphous silica left after kaolinite decomposition, assisted by the impurities. The cristobalite peaks were slightly shifted (22.06° *vs.* 21.984°). Small peaks with up to 14.5% intensity of $ZrSiO_4$ (ICDD 00-006-0266, body-centered tetragonal structure, I41/amd space group) were found with reasonable match (e.g., 27.04° *vs.* 26.979°). $ZrSiO_4$ formed from the reaction of SiO_2 from the clay and the monoclinic ZrO_2 raw material. Finally, small peaks (12.5% intensity) of leucite, $K_2O.Al_2O_3.4SiO_2$ or $KAlSi_2O_6$ (ICDD 00-038-1423, tetragonal structure, I41/a space group) with shifted peaks (e.g., 27.38° *vs.* 27.28°) was found due to the reaction by the K_2O impurity (0.91%) in the clay. Three small peaks at 18.34°, 22.90° and 23.66° remained unidentified with up to 2% background subtracted intensity.

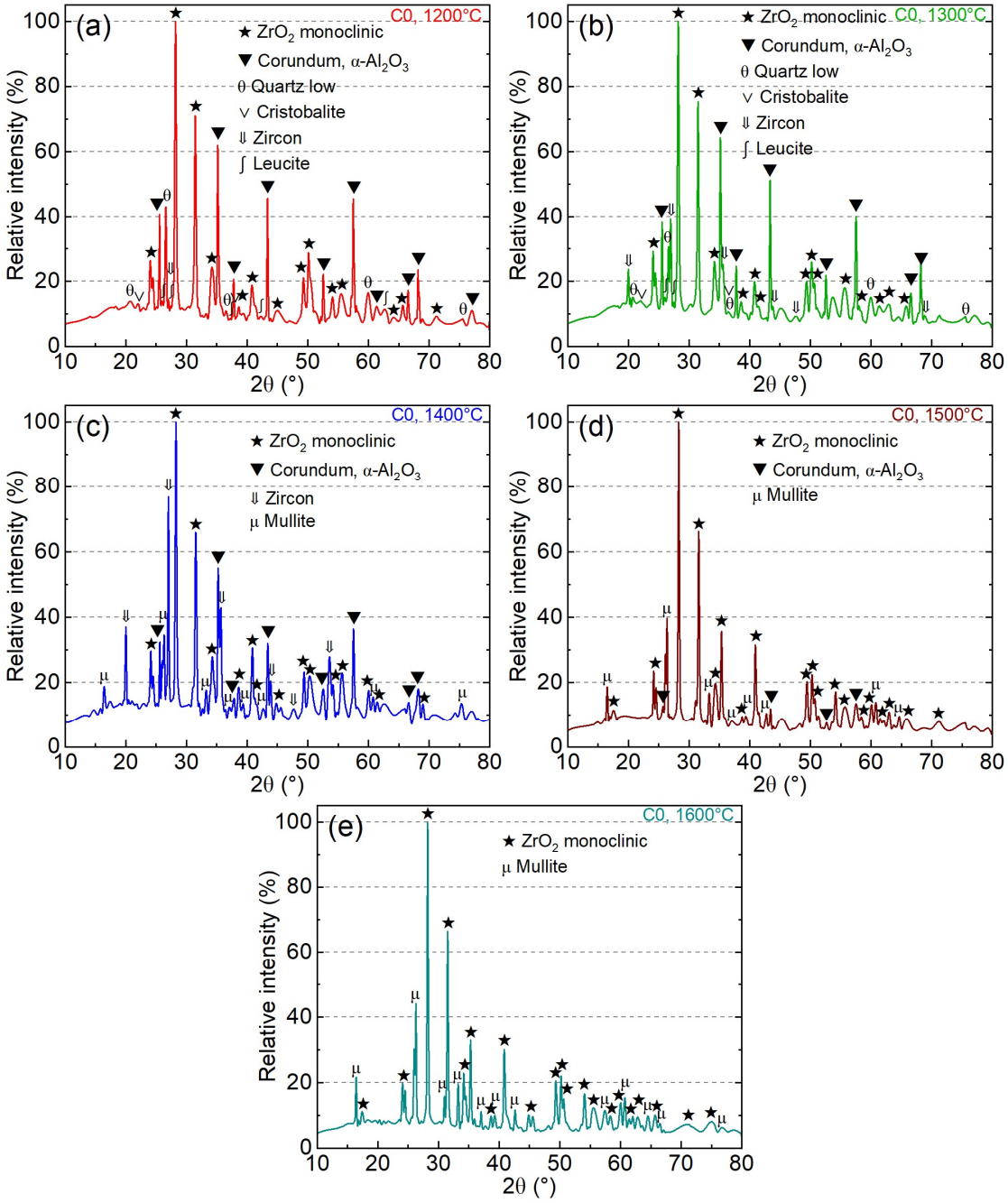

Figure 3. XRD patterns of C0 composition after firing for 2 h at (**a**) 1200 °C, (**b**) 1300 °C, (**c**) 1400 °C, (**d**) 1500 °C and (**e**) 1600 °C.

Monoclinic ZrO_2 continued to remain as the major phase in C0 from 1300 °C to 1600 °C (Figure 3b–e) with some variations in peak positions, e.g., 28.20°, 28.28°, 28.30° and 28.22°, respectively. From 1200 °C to 1300 °C, the intensities remained similar for α-Al_2O_3 (62.0 *vs.* 64.3%), cristobalite (13.1 *vs.* 13.9%) and leucite (12.5 *vs.* 13.5%). However, a reduction in the intensities of low quartz (43.0 *vs.* 30.6%) with a simultaneous increase in $ZrSiO_4$ (14.5 to 39.3%) was observed. 11 small peaks remained unidentified in C0 fired at 1300 °C with up to 2.3% background subtracted intensity. At 1400 °C, the leucite phase disappeared and probably formed glass, while both low quartz and cristobalite were fully consumed to form a large amount of $ZrSiO_4$ (76.8% intensity) along with the desirable mullite phase (ICDD 00-015-0776, orthorhombic structure, Pbam space group) with 34.7% intensity and a good 2θ match (26.32° *vs.* 26.267°). On the contrary, the intensity of α-Al_2O_3 decreased (64.3 *vs.* 55.1%). Three small unindexed peaks (≤2.9% background subtracted intensity) remained in C0 heated at 1400 °C. At 1500 °C, the $ZrSiO_4$ phase abruptly disappeared, which is in agreement with reports mentioning that the reaction of zircon and alumina to form zirconia and mullite progresses rapidly above 1500 °C according to Equation (1): [50]

$$2ZrSiO_4 + 3Al_2O_3 = 2ZrO_2 + 3Al_2O_3.2SiO_2 \quad (1)$$

This is an expansive reaction accompanied by de-densification [50]. Between 1400 °C and 1500 °C (Figure 3c,d), mullite slightly increased from 34.7% intensity to 39.7%, while the tallest corundum peak overlapped with monoclinic ZrO_2 and mullite and had a smaller intensity (55.1% *vs.* 35.6%). No other phases were present at 1500 °C, but two unidentified peaks with ≤3.3% background subtracted intensity remained. It was only at 1600 °C that the desirable ZM phase composition was formed, with mullite having 44.1% intensity. Hence, the reaction sequence was as follows. From the starting monoclinic ZrO_2-alumina-calcined clay mixture, the clay produced low quartz, cristobalite and leucite at 1200 °C. A small amount of $ZrSiO_4$ was formed due to the reaction between monoclinic ZrO_2, quartz and cristobalite. As the temperature increased to 1400 °C, the amount of $ZrSiO_4$ reached the maximum at the expense of the full consumption of low quartz and cristobalite. Leucite probably formed a liquid phase at this point. Mullite first appeared at 1400 °C. At 1500 °C, $ZrSiO_4$ suddenly dissociated, relinquishing silica, which reacted with corundum such that mullite increased with a simultaneous reduction in alumina. 1600 °C was high enough to fully react the α-Al_2O_3 to form mullite which remained stably with monoclinic ZrO_2. This reaction sequence is in reasonable agreement with other publications [9,37,51].

3.2. Phase Evolution of CaO Doped ZM Formulations

At the highest firing condition of 1650 °C for 2 h, C0 continued to be composed of monoclinic ZrO_2 and mullite (Figure 4a). With 1.77% calcite addition, which is expected to add 1.05% CaO, the intensities of monoclinic zirconia and mullite remained the same (Figure 4b). Still, partial stabilization of zirconia in tetragonal form with up to 7.7% intensity was found with a good match (e.g., 30.22° *vs.* 30.27°). Augmenting CaO to 2.11% (Figure 4c) caused a slight increase in the intensity of tetragonal ZrO_2 (8.9%), but the mullite peak intensity reduced from 36.1% to 26.8%. Simultaneously, a significant amount of α-Al_2O_3 appeared with 30.4% intensity. The added CaO seemed to react with mullite, leaching out its silica to form CaO-SiO_2 liquid phase and eutectic CaO-Al_2O_3-SiO_2 phases [2]. As the low-melting phases anorthite ($CaO.Al_2O_3.2SiO_2$) and gehlenite ($2CaO.Al_2O_3.SiO_2$) have $Al_2O_3/SiO_2 \leq 1$, while mullite ($3Al_2O_3.2SiO_2$) has 1.5, so, after reaction of mullite with CaO, the excess Al_2O_3 would be released and precipitated as corundum. Increasing CaO to 4.21% (C4 in Figure 4d) caused the complete dissolution of the silica in mullite, increasing α-Al_2O_3 to 34.9% intensity. A small cubic ZrO_2 (ICDD 00-049-1642, Fm-3m space group) peak with 7.9% intensity and reasonable match (29.96° *vs.* 30.12°) was detected. When CaO was increased to 7.37% (Figure 4e), the intensities of monoclinic ZrO_2, α-Al_2O_3 and cubic ZrO_2 remained consistent, and additionally, tetragonal ZrO_2 were also detected. Hence, C0 is ZM with monoclinic ZrO_2, while C1 contained partially stabilized tetragonal ZrO_2 which might benefit its fracture toughness. [42] The ZrO_2 partial stabilization continued in C2, but it was ZMA (ZrO_2-mullite-alumina) type aggregate. C4 and C7 were ZA aggregates with additional cubic ZrO_2 phases. The complete replacement of mullite by corundum in ZM compositions has also been reported when 10 wt% CaO is doped [41]. As corundum is harder than mullite, conversion of ZM into ZA may enhance its wear resistance [52], making it potentially suitable for producing wear-resistant tiles.

Based on the estimated "after firing" compositions in Table 2, their phase evolution was further thermodynamically evaluated by FactSage simulations and shown in Figure 5. The C0 composition at 1650 °C was predicted to contain 56.9 wt% mullite, 38.5% tetragonal ZrO_2 and 4.6% liquid phase arising mainly from the impurities in the clay. However, when this sample's XRD was done at room temperature (Figure 4a), in the absence of a stabilizer, the tetragonal ZrO_2

is expected to have transformed back to the monoclinic phase. Additionally, monoclinic ZrO_2 showed stronger XRD intensity than mullite despite being the secondary phase (per FactSage). Rietveld refinement (which was not available during the time of this study) would have corrected the intensity and provided a better XRD phase quantification.

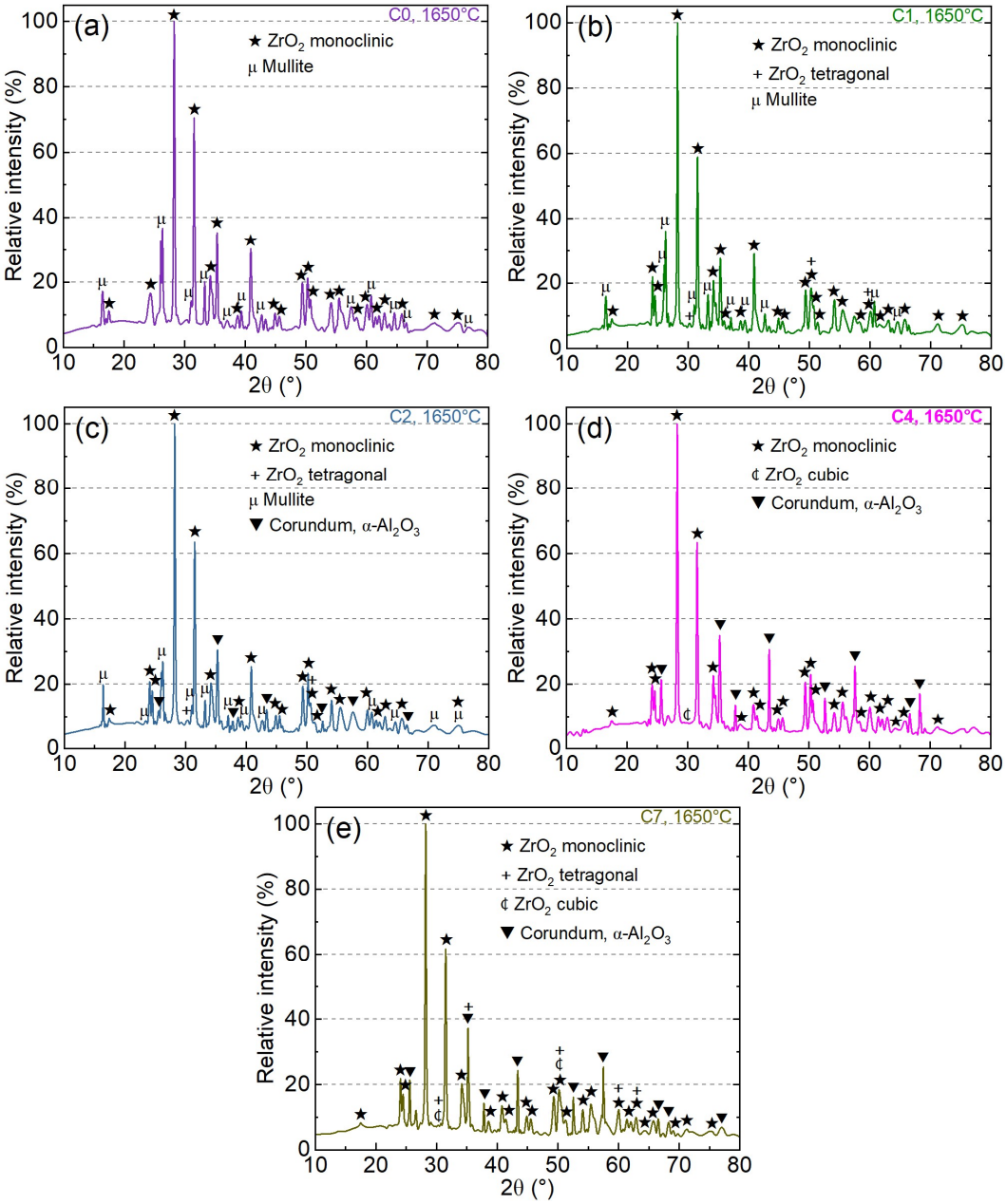

Figure 4. XRD patterns of ZrO_2-mullite formulations fired for 2 h at 1650 °C containing different amounts of CaO: (**a**) 0%, (**b**) 1.05%, (**c**) 2.11%, (**d**) 4.21% and (**e**) 7.37%.

Figure 5a shows that the range of CaO additions (0–7.37 wt%) in this investigation on ZM covered the entire region of stability of the mullite phase which is eventually dissolved in the rapidly forming liquid phase. For C1, C2, C4 and C7, the mullite dramatically reduced to 49.2, 39.6, 15.3 and 0 wt%, while tetragonal ZrO_2 did not have sufficient solubility in the liquid phase and lowered slowly to 37.1, 35.6, 32.8 and 29.4 wt%, respectively. 0.2–0.8 wt% leucite was predicted by FactSage in C1 to C4, while it was only detected by XRD in C0 at 1200 and 1300 °C (Figure 3a,b) arising from the K_2O impurity in the clay. Whereas thermodynamic calculations simulated mullite to disappear only in C7, experimentally, XRD showed mullite was lost in both C4 and C7. Cubic ZrO_2 was also not predicted, but it was found at the higher CaO levels in C4 and C7. Differences between FactSage and experimental results can occur due to slow reaction kinetics caused by the use of relatively coarser particles, times not long enough to achieve equilibrium and slower cooling that can exsolve part of the solid solutions [29,48] like the stabilizer in ZrO_2. Due to the dissolution of the mullite phase, corundum was produced, and its quantity predicted by FactSage in C2, C4 and C7 were 1.4, 9.9 and 11.1 wt%, which qualitatively matches the XRD results in Figure 4c–e. Finally, it was observed that as the CaO

content in ZM formulation increased from 0, 1.05, 2.11, 4.21 to 7.37%, the liquid phase content rose dramatically as 4.6, 13.5, 22.7, 41.5 and 59.4 wt%. This was concomitant with a drastic drop in the fluid viscosity from 6.3 Pa·s in C0 to 0.3–0.6 Pa.s in C1–C7 (Figure 5b). Thus, moderate amounts of CaO doping in a ZM formulation produced copious amounts of a very fluid (watery) liquid phase that changes its phase assemblage towards ZA.

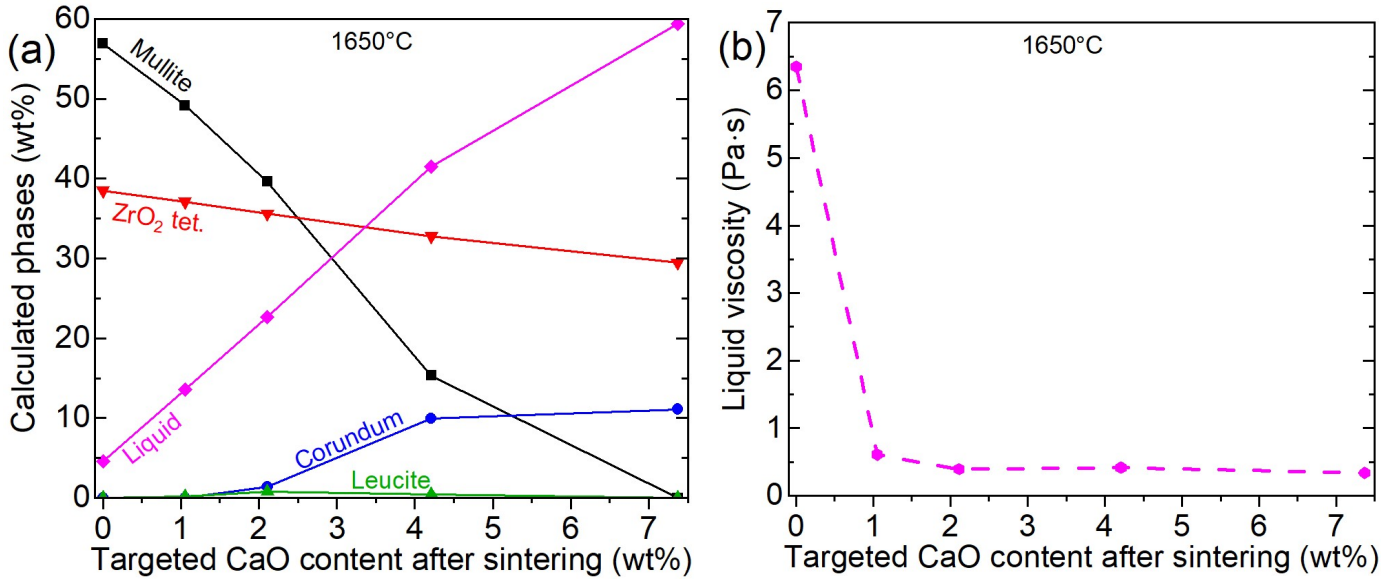

Figure 5. FactSage thermodynamic equilibrium calculations predicting (**a**) phases formed and (**b**) viscosity of the liquid phase in the compositions C0, C1, C2, C4 and C7 at the firing temperature of 1650 °C.

3.3. Densification

The undoped ZM composition C0 had the least quantity and the highest viscosity of the liquid phase at 1650 °C (Figure 5). Hence, at 1550 °C, it had hardly sintered and exhibited a low bulk density of 2.54 g/cm^3 and a high apparent porosity of 29.0% (Figure 6). With increasing firing temperature to 1650 °C, C0 only slightly sintered and had an open porosity of 26.5%. This exemplifies the well-known difficulty in sintering zirconia-mullite compositions [25] with a particle size (e.g., <75 µm) common for the refractory brick matrix and for making refractory raw material aggregates which is coarser than the submicron sizes typically reported in the literature [3,4,31,32]. This motivates the need for a mineralizer in the current study. CaO incorporation into ZM assisted densification by liquid phase sintering up to 4.21% dopant level as the apparent porosity at 1550 °C dropped from 29% for C0 through 20% for C2 to 0.7% for C4. C4 also had the highest bulk density of 3.00 g/cm^3. As only C0 and C1 had ZM phase composition after firing, while C2 formed monoclinic zirconia + mullite + corundum (ZMA), while C4 and C7 evolved into ZA, so the lowest porosity achieved in a ZM aggregate in this study was for C1 at 1650 °C (22.7%). As this is too high compared to ~3% open porosity for typical refractory aggregates [8,11,30], so no "true ZM" aggregate could be developed in this study that was dense enough. The optimally dense aggregate in this study was C4 fired at 1550 °C with a ZA phase composition, and it can be rated to a maximum application temperature of 1550 °C, as above that it showed detrimental effect from the liquid phase. Appropriate amount and viscosity of liquid phase benefits sintering and is manifested as increasing density with a rise in sintering temperature as in the case for C0, C1 and C2. However, for C4, as the temperature increased from 1550 °C to 1650 °C, the bulk density surprisingly reduced from 3.00 g/cm^3 to 2.89 g/cm^3. It was found that the weight loss of the C4 pellets after firing at 1550, 1600 and 1650 °C were 3.8, 5.0 and 17.0%, respectively, which indicates that at the highest sintering temperature, the glassy phase drained out of the sample. As the apparent porosity stayed almost the same (0.2–0.3%) for C4 at 1600–1650 °C, excessive liquid phase formation likely caused a drop in its true specific gravity at first, which then oozed out and left behind closed porosity thereby reducing the bulk density. For C7, the liquid phase content was so high and had such low viscosity that it percolated out and left the solid ceramic grain structure at 1550 °C with a high open porosity (30.7%), which means that the temperature was not sufficiently high to sinter the remnant material. With increasing firing temperature, the glass-depleted C7 sintered to attain 3.9 and 0.5% open porosity for 1600 °C and 1650 °C, respectively. The weight losses of C7 pellets during firing between 1550–1650 °C were 5.6, 13.8 and 32.0%, which shows that the liquid phase became thinner, and its quantity increased at higher temperatures, seeped down the samples, and fortunately, the temperatures were appropriately high to densify the leftover zirconia and alumina. However, such kind of liquid phase loss is not suitable for industrial production of

ceramics. Until the glassy phase stayed within the sample, it can be said that the phase changes in the samples influenced its densification, but it was the large amount and low viscosity of the glassy phase which likely dominated the overall sintering.

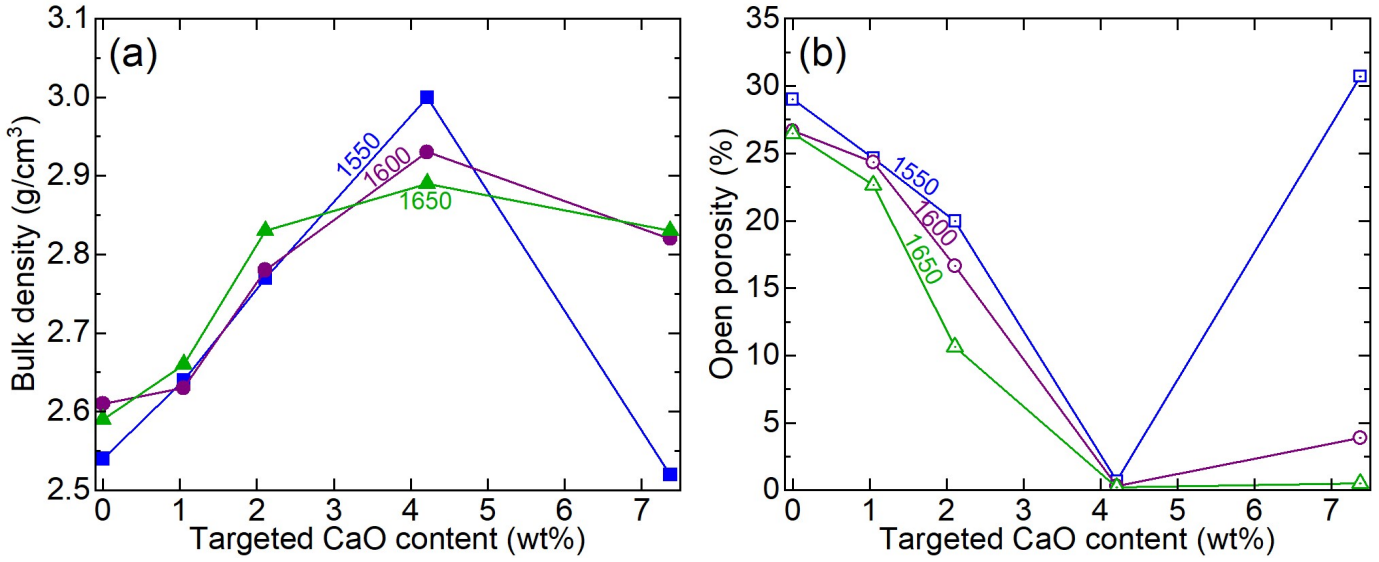

Figure 6. Impact of CaO doping on (**a**) bulk density and (**b**) open porosity of ZM formulations at three sintering temperatures.

3.4. Microstructure

As C0 fired at 1650 °C for 2 h had 26.5% open porosity, its microstructure (Figure 7) consisted of patches of pores. The fracture surface images (Figure 7a,b) show that the darker mullite phase was present as groups of somewhat equiaxed, small grains, which are likely to be primary mullite [53,54] along with several interlocked elongated rod-like grains (0.9 ± 0.2 µm thickness) which are believed to be secondary mullite. The presence of two types of mullite morphology is common when the precursor is a kaolinite-alumina mixture [55]. The lighter small monoclinic ZrO_2 grains (2.5 ± 1.1 µm) were found to be scattered around the darker mullite phase, as well as occur as large clusters of direct bonded ZrO_2 grains (Figure 7b). Such coalescence and clustering of the ZrO_2 grains were observed in ZM prepared by Wei et al. [37]. ZrO_2 grain clusters are also reported when ZM forms from the reaction of $ZrSiO_4$ and Al_2O_3 [56], as in this study where in situ $ZrSiO_4$ is formed at intermediate firing temperatures. However, it was only with point EDS and elemental mapping of polished surfaces using the Zeiss SEM (Figure 7 c–f) that the phases could be identified with certainty. The round and oval ZrO_2 grains did not contain any other element, and in the absence of solid solution forming cations it remained as monoclinic ZrO_2 as earlier confirmed by XRD. Both the cuboidal primary mullite and the thin rod-like secondary mullite did not contain any Zr or Ca and had an average at% Al/Si ratio of 2.0 ± 0.4 compared to 3.0 for mullite ($3Al_2O_3.2SiO_2$). The lack of ZrO_2 solid solution in mullite is reasonably expected as it has very little (1%) solubility [31,57].

The microstructure of C1 (Figure 8) appeared denser than C0. The cuboidal primary mullite grains appeared larger and many grains had sharp edges. There was a slight increase in the size of the zirconia grains (3.5 ± 1.3 µm) and the thickness of the secondary mullite rods (1.7 ± 0.4 µm). The Ca elemental map coincided more with Si and Al than Zr, suggesting that the CaO dopant reacted more with the mullite-forming liquid phase than to stabilize the monoclinic ZrO_2. Point EDS revealed that the round zirconia phase (Z) was devoid of Ca (stabilizer). The thin secondary mullite rods had an Al/Si at% ratio of 1.8 with 0.17 at% Ca.

The microstructure of C2 (Figure 9) appeared to be significantly denser, and the pores were smaller and more uniformly distributed. The cuboidal primary mullite appeared larger with sharp boundaries and sometimes had a rhombus morphology. The secondary mullite rods were significantly longer and thicker (2.8 ± 0.6 µm) than before and had sharp edges. A small number of thin mullite rods were also present. The alumina phase appeared both as tiny round grains and short, thick rods with rounded edges. The bright zirconia clusters had disintegrated, and dispersed grains (3.7 ± 1.0 µm) were seen with potentially glassy phases between them. Point EDS revealed that the zirconia grains contained no Ca, while the cuboidal primary mullite grains had an Al/Si at% ratio of 2.6 with 0.09 at% Ca. The thick secondary mullite rods had an Al/Si ratio of 2.1 with 0.59 at% Ca, suggesting its interaction with the liquid phase. The thick alumina rods were pure with only 0.01 at% Si.

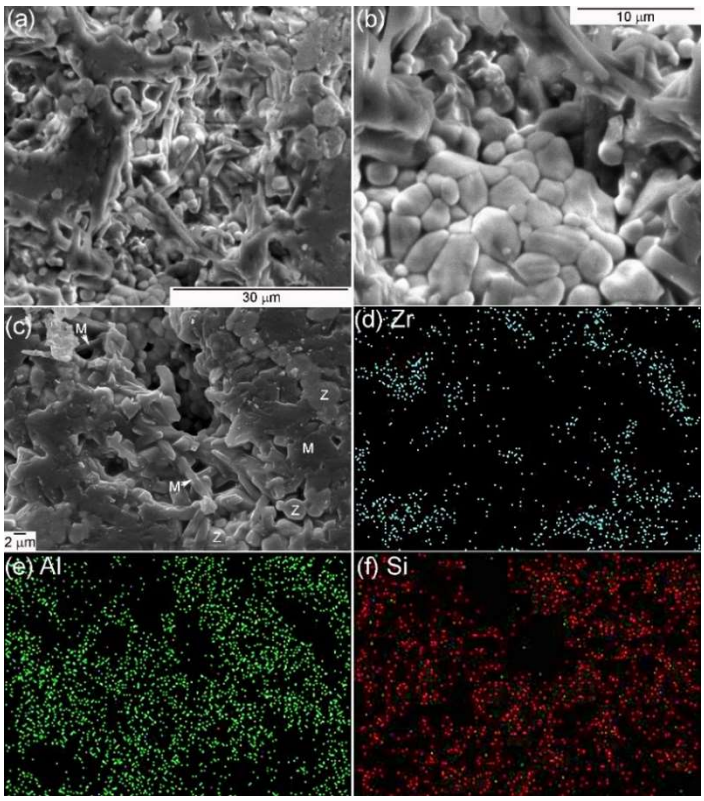

Figure 7. (**a**,**b**) Fracture surface secondary electron images captured by the FEI SEM and (**c**–**f**) polished surface images and elemental mapping using Zeiss SEM of C0 sintered at 1650 °C. The markers for zirconia (Z) and mullite (M) have been placed only where point EDS was done.

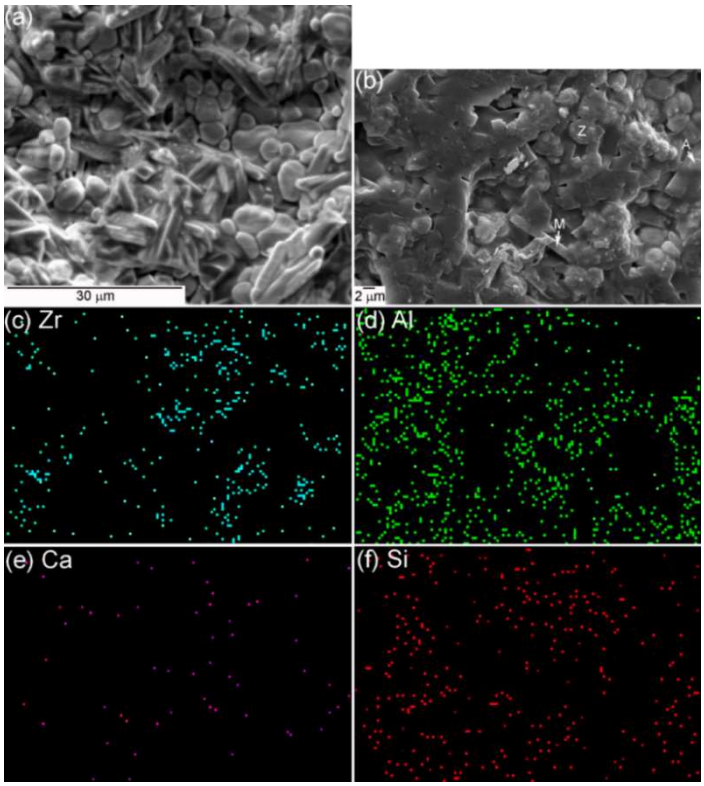

Figure 8. (**a**) Fracture surface SEM image and (**b**) polished surface micrographs along with (**c**–**f**) elemental maps of C1 after sintering at 1650 °C. The markers for zirconia (Z), mullite (M) and alpha alumina (A) have been placed only where point EDS was done.

As C4 was characterized by the complete replacement of mullite by alumina (Figure 4d), its microstructure did not have any long, thick mullite rods (Figure 10). Instead, short, interlinked alumina rods of varying thicknesses (primarily 1.2 ± 0.3 μm, and occasionally 2.7 ± 0.7 μm) were observed, along with some tiny, round alumina grains. The pores were concentrated near alumina rods, confirming that the $CaO\text{-}SiO_2\text{-}Al_2O_3$ liquid phase drained out of the composite at

1650 °C, leaving closed pores behind. The zirconia grains became larger in size (4.0 ± 1.7 μm) and were mostly separated by a glassy phase. The Ca elemental maps overlapped with both Zr, Si and Al, suggesting that it helped stabilize zirconia and formed liquid phase. The ZrO_2 grains had an average of 0.26 at% Ca and 0.40% Al. The Al_2O_3 rods contained 0.08% Ca and 0.77% Si.

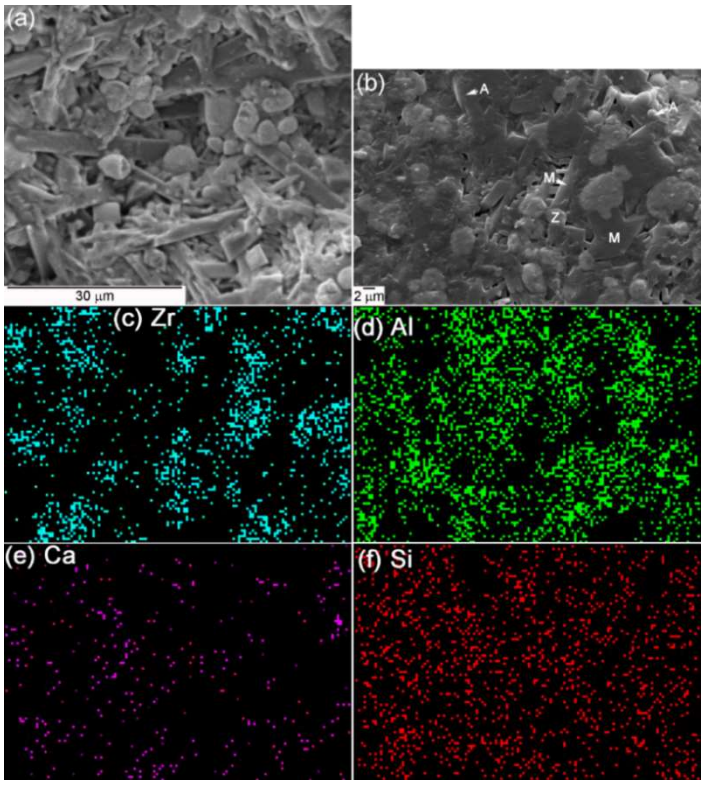

Figure 9. (**a**) Fracture surface SEM image and (**b**) polished surface micrographs along with (**c**–**f**) elemental maps of C2 after sintering at 1650 °C. The markers for zirconia (Z), mullite (M) and alpha alumina (A) have been placed only where point EDS was done.

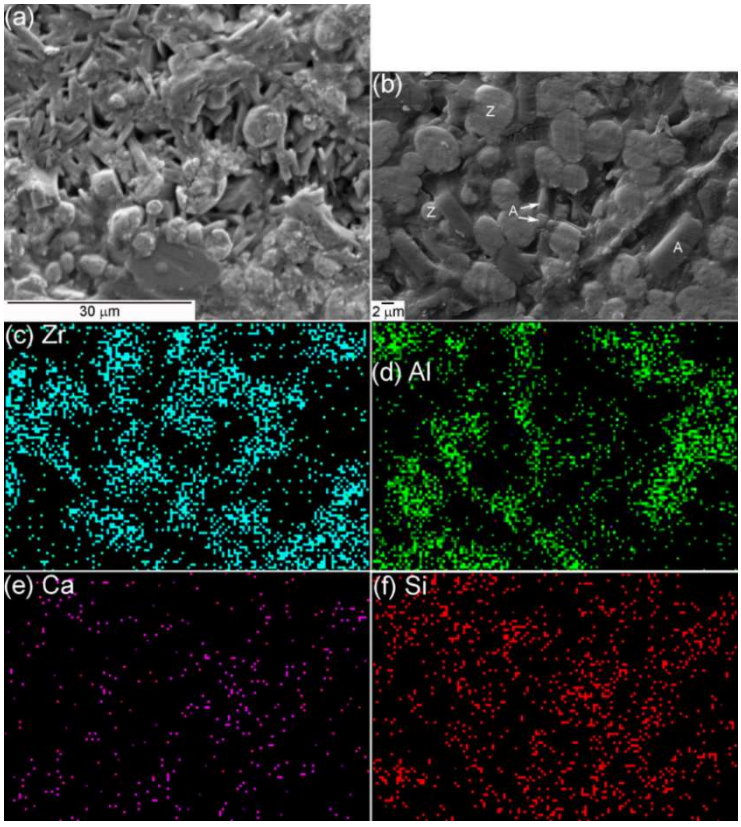

Figure 10. (**a**) Fracture surface SEM image and (**b**) polished surface micrographs along with (**c**–**f**) elemental maps of C4 after sintering at 1650 °C. The markers for zirconia (Z) and alpha alumina (A) have been placed only where point EDS was done.

The microstructure of C7 (Figure 11) consisted of a smaller number of thin alumina rods (0.7 ± 0.1 µm) with a significant amount of glass with 13.0 at% Ca and an Al/Si ratio of 0.94 which is close to anorthite (1.0). Some thin rods with a similar composition to the anorthite-like glass had 6.9 at% Ca and an Al/Si ratio of 0.72. XRD did not detect Anorthite, but it is possible that its amount was so small that XRD could not detect it, but EDS found it. The ZrO_2 grains were the largest (6.5 ± 1.9 µm) and were abundantly surrounded by glass and had 0.07% Ca and 1.0% Si, which could be from the EDS X-ray interaction volume at 20 kV interacting with the adjacent glass. It had been observed in other studies also that in high CaO-doped compositions, the CaO rather reacts with Al_2O_3 and SiO_2, forming anorthite and glassy phases, than going into a solid solution with ZrO_2 [43].

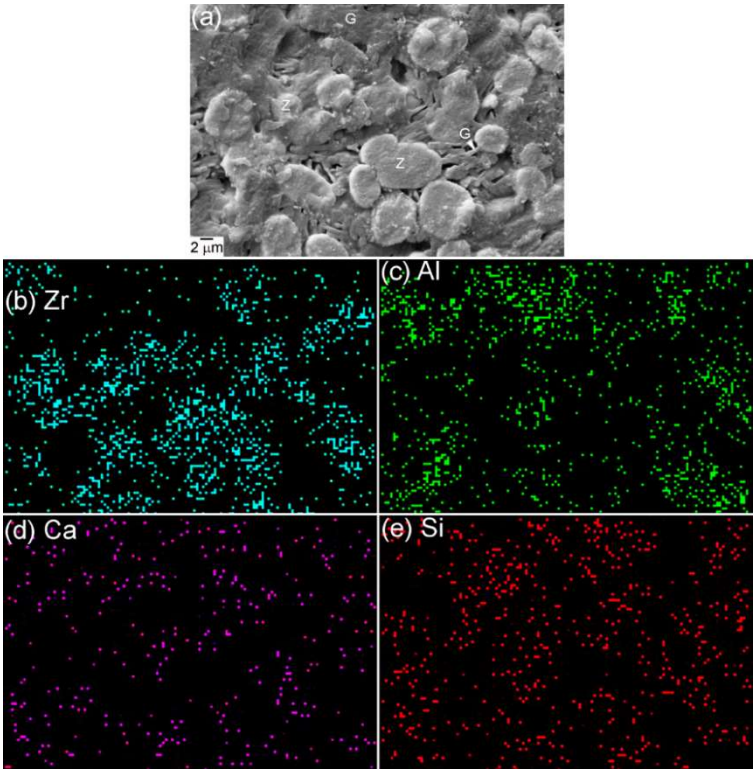

Figure 11. (**a**) Polished surface micrographs along with (**b**–**e**) elemental maps of C7 after sintering at 1650 °C. The markers for zirconia (Z) and glass (G) have been placed only where point EDS was done.

4. Conclusions

The feasibility of preparing an alternative of fused zirconia mullite (37.4 wt% ZrO_2) refractory aggregate or matrix was explored using conventional sintering and low-cost siliceous clay mixed with calcined alumina and monoclinic ZrO_2. At 1200 °C, low quartz and cristobalite from the clay reacted with ZrO_2 to form $ZrSiO_4$, which remained along with monoclinic ZrO_2, α-Al_2O_3 and traces of leucite. The amount of $ZrSiO_4$ peaked at 1400 °C, while at 1500 °C, it abruptly and completely dissociated, increasing the amount of mullite, while traces of unreacted α-Al_2O_3 still remained. A minimum firing temperature of 1600 °C was necessary to obtain the desirable phase composition of mullite + monoclinic ZrO_2 (ZM). However, this contained a high open porosity (26.5%) after firing at 1650 °C for 2 h despite having 4.6 wt% liquid phase (from FactSage). Its microstructure consisted of small equiaxed primary mullite grains, rod-like secondary mullite (0.9 µm thick), and scattered and clustered ZrO_2 grains. In order to densify and attain partial stabilization of the monoclinic ZrO_2, calcite was added. With 1.05% CaO, some tetragonal ZrO_2 formed, but still 22.7% open porosity remained after firing at 1650 °C for 2 h, although 13.5% liquid phase formed with a low viscosity (0.6 Pa·s) in this composite. With 2.11% CaO addition, mullite partly dissolved forming α-Al_2O_3 (ZMA aggregate), which still had 10.7% apparent porosity, underscoring the difficulty in conventional sintering of ZM formulations with <75 µm particle size. CaO doping to this level also increased the thickness of the secondary mullite rods up to 2.8 µm and the enlargement of the ZrO_2 grains up to 3.7 µm. EDS revealed that CaO mostly remained in the intergranular glassy phase rather than inside the ZrO_2 grains.

Mullite was unfortunately lost with 4.21% CaO doping but favorably formed some cubic ZrO_2 and attained a low porosity of 0.7% with 3.00 g/cm^3 bulk density after firing at 1550 °C for 2 h. This ZA aggregate is limited to 1550 °C application temperature as beyond that, the excess liquid phase drained out, forming closed pores and the aggregate lost

bulk density. The α-Al_2O_3 phase was present as interlinked rods, 1.2–2.7 μm thick, and the Ca reached 0.26 at% inside the ZrO_2 grains. 7.37% CaO addition was detrimental as it formed an excess liquid phase that drained out at 1550 °C with 5.6% weight loss. At 1650 °C, the weight loss was 32.0%, the alumina rods had become thinner (0.7 μm), and the glass composition was similar to anorthite with possibly some small, thin anorthite rods. The ZrO_2 phase exhibited steady grain growth to 6.5 μm. This work recommends that in refractory castables with ZM aggregates, the calcium aluminate cement binder content should be restricted to a final CaO content of under 2.1% to avoid partial dissolution of mullite. Overall, it can be inferred that out of the two main cost-effective stabilizers for ZrO_2 in ZrO_2-mullite for refractories, neither CaO (in this study) nor MgO (ref. [40]) is truly suitable for simultaneously attaining stabilization and densification.

Acknowledgments

The authors express sincere gratitude to A. S. K. Sinha for providing XRF analysis, Bhagmal Singh for operating XRD, Debarpita Paul (Oklahoma State University, USA) for assisting in XRD data analysis, Tristan Eisenbraun (Vesuvius Research) for processing sintering data, Ashish Tripathi and the staff at the Central Instrument Facility (IITBHU) for operating SEM-EDS. S.M. and H.A. are grateful to the Ministry of Human Resource Development, India, for providing scholarships during their Masters. The funds from The National Centre for Research and Development, grant no. LIDER/14/0086/L-12/20/NCBR/2021, and from the "Research project Excellence initiative—research university" from the AGH University grant ID9053 are acknowledged.

Author Contributions

Conceptualization, S.M. and D.K.; Methodology, S.M.; Software, S.M., I.J. and H.A.; Validation, S.M.; Formal Analysis, S.M.; Investigation, S.M., H.A., A.P. and P.G.; Resources, D.K. and O.P.; Data Curation, S.M. and H.A.; Writing—Original Draft Preparation, S.M.; Writing—Review & Editing, S.M., I.J., A.P. and H.A.; Visualization, S.M., I.J. and H.A. Supervision, S.M., D.K. and O.P.; Project Administration, D.K. and O.P.

Ethics Statement

Not applicable as this study did not involve humans or animals.

Informed Consent Statement

Not applicable as this study did not involve humans.

Funding

This research received no external funding.

Declaration of Competing Interest

The authors declare that they have no known competing financial interests or personal relationships that could have appeared to influence the work reported in this paper.

References

1. Schneider H, Komarneni S. (Eds.) *Mullite*; Wiley-VCH Verlag GmbH: Weinheim, Germany, 2005. doi:10.1002/3527607358.
2. Schacht CA. *Refractories Handbook*; Marcel Dekker: New York, NY, USA, 2004. doi:10.1201/9780203026328.
3. Moya JS, Osendi MI. Microstructure and Mechanical Properties of mullite/ZrO_2 composites. *J. Mater. Sci.* **1984**, *19*, 2909–2914. doi:10.1007/BF01026966.
4. Torrecillas R, Moya JS, De Aza S, Gros H, Fantozzi G. Microstructure and mechanical properties of mullite-zirconia reaction-sintered composites. *Acta Metall. Mater.* **1993**, *41*, 1647–1652. doi:10.1016/0956-7151(93)90184-T.
5. Yuan Q-M, Tan J-Q, Jin Z-G. Preparation and Properties of Zirconia-Toughened Mullite Ceramics. *J. Am. Ceram. Soc.* **1986**, *69*, 265–267. doi:10.1111/j.1151-2916.1986.tb07422.x.
6. Prusty S, Mishra DK, Mohapatra BK, Mishra G, Singh SK. Preparation of fused zirconia/mullite aggregates from sillimanite, zircon, and alumina mixtures via plasma. *J. Am. Ceram. Soc.* **2012**, *95*, 530–537. doi:10.1111/j.1551-2916.2011.04898.x.
7. Takenami M, Akamine K. Zirconia-Mullite Refractory Raw Material and a Plate Brick, US 8,138,109 B2, 2009. Available online: https://patents.google.com/patent/US8138109B2/en (accessed on 4 August 2024).
8. Imerys, ALODUR FZM by Imerys Refractory Minerals. Available online: https://www.imerys.com/product-ranges/alodur-

refractories (accessed on 3 August 2024).
9. Zanelli C, Dondi M, Raimondo M, Guarini G. Phase composition of alumina-mullite-zirconia refractory materials. *J. Eur. Ceram. Soc.* **2010**, *30*, 29–35. doi:10.1016/j.jeurceramsoc.2009.07.016.
10. Aksel C. The microstructural features of an alumina-mullite-zirconia refractory material corroded by molten glass. *Ceram. Int.* **2003**, *29*, 305–309. doi:10.1016/S0272-8842(02)00137-2.
11. DURAMUL ZR from Washington Mills. Available online: https://www.washingtonmills.com/products/fused-mullite/duramul-zr (accessed on 4 August 2024).
12. Bigeard A, Vespa P, Leplay P, Mesnager C, Citti O, Bouvard D, et al. Thermomechanical behavior of an alumina-mullite-zirconia refractory ceramic: Sintering and thermally induced damage. *J. Eur. Ceram. Soc.* **2024**, *44*, 1256–1266. doi:10.1016/j.jeurceramsoc.2023.09.051.
13. Manfredo LJ, McNally RN. The corrosion resistance of high ZrO_2 fusion-cast Al_2O_3-ZrO_2-SiO_2 glass refractories in soda lime glass. *J. Mater. Sci.* **1984**, *19*, 1272–1276. doi:10.1007/BF01120038.
14. Asokan T. Microstructural features of fusion cast Al_2O_3-ZrO_2-SiO_2 refractories. *J. Mater. Sci. Lett.* **1994**, *13*, 343–345. doi:10.1007/BF00420793.
15. Rendtorff N, Garrido L, Aglietti E. Mullite-zirconia-zircon composites: Properties and thermal shock resistance. *Ceram. Int.* **2009**, *35*, 779–786. doi:10.1016/j.ceramint.2008.02.015.
16. DURAZON CSG from Washington Mills. Available online: https://www.washingtonmills.com/products/zirconia/durazon-csg (accessed on 4 August 2024).
17. Calcia Stabilized Zirconia from Foskor Zirconia. Available online: https://www.foskor-zirconia.com/CalciaStabilizedZirconia.html (accessed on 4 August 2024).
18. Morris M, Wagner RJ. Alumina-Zirconia Refractory Material and Articles Made Therefrom, EP0755366A1, 1995. Available online: https://patents.google.com/patent/EP0755366A1/en (accessed on 4 August 2024).
19. Yugeswaran S, Selvarajan V, Dhanasekaran P, Lusvarghi L. Transferred arc plasma processing of mullite-zirconia composite from natural bauxite and zircon sand. *Vacuum* **2009**, *83*, 353–359. doi:10.1016/j.vacuum.2008.05.033.
20. Bhattacharjee S, Singh SK, Galgali RK. Preparation of zirconia toughened mullite by thermal plasma. *Mater. Lett.* **2000**, *43*, 77–80. doi:10.1016/S0167-577X(99)00234-7.
21. Yoshimura M, Kaneko M, Somiya S. Rapid quenching of melts in the system ZrO_2-SiO_2-Al_2O_3. *J. Phys. Colloq.* **1986**, *47*, 473–477. doi:10.1051/jphyscol:1986171.
22. Khor KA, Yu LG, Li Y, Dong ZL, Munir ZA. Spark plasma reaction sintering of ZrO_2- mullite composites from plasma spheroidized zircon/alumina powders. *Mater. Sci. Eng. A* **2003**, *339*, 286–296. doi:10.1016/S0921-5093(02)00151-X.
23. Bodhak S, Bose S, Bandyopadhyay A. Densification study and mechanical properties of microwave-sintered mullite and mullite-zirconia composites. *J. Am. Ceram. Soc.* **2011**, *94*, 32–41. doi:10.1111/j.1551-2916.2010.04062.x.
24. Ko H-D, Lin C-C. Oxygen diffusivities in mullite/zirconia composites measured by 18O/16O isotope exchange and secondary ion mass spectrometry. *J. Mater. Res.* **2008**, *23*, 353–358. doi:10.1557/jmr.2008.0073.
25. Yuan Q, Tan J, Shen J, Zhu X, Yang Z. Processing and Microstructure of Mullite-Zirconia Composites Prepared from Sol-Gel Powders. *J. Am. Ceram. Soc.* **1986**, *69*, 268–269. doi:10.1111/j.1151-2916.1986.tb07423.x.
26. Orange G, Fantozzi G, Cambier F, Leblud C, Anseau MR, Leriche A. High temperature mechanical properties of reaction-sintered mullite/zirconia and mullite/alumina/zirconia composites. *J. Mater. Sci.* **1985**, *20*, 2533–2540. doi:10.1007/BF00556085.
27. Mandal S, Mondal S, Das K. Microstructure and phase evolution of Indian magnesite-derived $MgAl_2O_4$ as a function of stoichiometry and ZrO_2 doping. *Int. J. Appl. Ceram. Technol.* **2018**, *15*, 161–170. doi:10.1111/ijac.12759.
28. Mandal S, Mahapatra MK. Use of dilatometer to screen refractory raw materials. *Int. J. Ceram. Eng. Sci.* **2022**, *4*, 47–52. doi:10.1002/ces2.10113.
29. Mandal S, Hemrick JG, Mahapatra MK. Impact on aggregate / matrix bonding when a refractory contains zinc aluminate instead of spinel and magnesia-chrome. *J. Am. Ceram. Soc.* **2023**, *106*, 5662–5678. doi:10.1111/jace.19214.
30. Mandal S, Hemrick JG, Mahapatra MK. Zinc aluminate ($ZnAl_2O_4$) refractory aggregates: Dilatometric sintering studies and thermal expansion coefficient. *J. Eur. Ceram. Soc.* **2022**, *42*, 6244–6254. doi:10.1016/j.jeurceramsoc.2022.06.058.
31. Koyama T, Hayashi S, Yasumori A, Okada K. Preparation and characterization of mullite-zirconia composites from various starting materials. *J. Eur. Ceram. Soc.* **1994**, *14*, 295–302. doi:10.1016/0955-2219(94)90066-3.
32. Ebadzadeh T, Ghasemi E. Influence of starting materials on the reaction sintering of mullite-ZrO_2 composites. *Mater. Sci. Eng. A* **2000**, *283*, 289–297. doi:10.1016/S0921-5093(99)00631-0.
33. Ebadzadeh T, Ghasemi E. Effect of TiO_2 addition on the stability of t-ZrO_2 in mullite-ZrO_2 composites prepared from various starting materials. *Ceram. Int.* **2002**, *28*, 447–450. doi:10.1016/S0272-8842(01)00117-1.
34. Chandra D, Das GC, Sengupta U, Maitra S. Studies on the reaction sintered zirconia-mullite-alumina composites with titania as additive. *Ceramica* **2013**, *59*, 487–494. doi:10.1590/S0366-69132013000300021.
35. Haldar MK, Pal TK, Banerjee G. Preparation and properties of Y_2O_3 containing zirconia-mullite composites derived from sillimanite beach sand. *Ceram. Int.* **2002**, *28*, 311–318. doi:10.1016/S0272-8842(01)00096-7.

36. Das K, Mukherjee B, Banerjee G. Effect of yttria on mechanical and microstructural properties of reaction sintered mullite-zirconia composites. *J. Eur. Ceram. Soc.* **1998**, *18*, 1771–1777. doi:10.1016/s0955-2219(98)00095-8.
37. Wei WCJ, Kao HC, Lo MH. Phase Transformation and Grain Coarsening of Zirconia/Mullite Composites. *J. Eur. Ceram. Soc.* **1996**, *16*, 239–247. doi:10.1016/0955-2219(95)00157-3.
38. Wu JM, Lin CM. Effect of CeO_2 on reaction-sintered mullite-ZrO_2 ceramics. *J. Mater. Sci.* **1991**, *26*, 4631–4636. doi:10.1007/BF00612398.
39. Das K, Banerjee G. Mechanical properties and microstructures of reaction sintered mullite-zirconia composites in the presence of an additive—Dysprosia. *J. Eur. Ceram. Soc.* **2000**, *20*, 153–157. doi:10.1016/S0955-2219(99)00147-8.
40. Haldar MK. Effect of magnesia additions on the properties of zirconia-mullite composites derived from sillimanite beach sand. *Ceram. Int.* **2003**, *29*, 573–581. doi:10.1016/S0272-8842(02)00204-3.
41. Chandra D, Das G, Maitra S. Comparison of the Role of MgO and CaO Additives on the Microstructures of Reaction-Sintered Zirconia-Mullite Composite. *Int. J. Appl. Ceram. Technol.* **2015**, *12*, 771–782. doi:10.1111/ijac.12263.
42. Pena P, Miranzo P, Moya JS, De Aza S. Multicomponent toughened ceramic materials obtained by reaction sintering—Part 1 ZrO_2-Al_2O_3-SiO_2-CaO system. *J. Mater. Sci.* **1985**, *20*, 2011–2022. doi:10.1007/BF01112284.
43. Miranzo P, Pena P, De Aza S, Moya JS, Rincon JM, Thomas G. TEM study of reaction-sintered zirconia-mullite composites with CaO and MgO additions. *J. Mater. Sci.* **1987**, *22*, 2987–2992. doi:10.1007/BF01086502.
44. Zhang A, Kang L, Zhang Y, Ding D, Zhang Y. Thermal behaviors and kinetic analysis of two natural kaolinite samples selected from Qingshuihe region in Inner Mongolia in China. *J. Therm. Anal. Calorim.* **2021**, *145*, 3281–3291. doi:10.1007/s10973-020-09869-4.
45. Keller WD. The Sedimentology of Flint Clay. *J. Sediment. Res.* **1981**, *51*, 233–244. doi:10.1306/212F7C57-2B24-11D7-8648000102C1865D.
46. Sahnoune F, Belhouchet H, Saheb N, Heraiz M, Chegaar M, Goeuriot P. Phase transformation and sintering behaviour of mullite and mullite-zirconia composite materials. *Adv. Appl. Ceram.* **2011**, *110*, 175–180. doi:10.1179/1743676111Y.0000000004.
47. Jastrzębska I, Piwowarczyk A, Błachowski A, Mandal S. Influence of PbO/CuO ratio on phase composition, microstructure, melt wettability and recyclability of copper slag. *Ceram. Int.* **2024**, *50*, 23315–23330. doi:10.1016/j.ceramint.2024.04.055.
48. Mandal S, Kumar CJD, Kumar D, Syed K, Van Ende MA, Jung IH, et al. Designing environment-friendly chromium-free Spinel-Periclase-Zirconia refractories for Ruhrstahl Heraeus degasser. *J. Am. Ceram. Soc.* **2020**, *103*, 7095–7114. doi:10.1111/jace.17402.
49. ASTM International. *C20-00 Standard Test Methods for Apparent Porosity, Water Absorption, Apparent Specific Gravity, and Bulk Density of Burned Refractory Brick and Shapes by Boiling Water*; ASTM: West Conshohocken, PA, USA, 2015. doi:10.1520/C0020-00R15.
50. Claussen N, Jahn J. Mechanical properties of sintered, in situ-reacted mullite-zirconia composites. *J. Am. Ceram. Soc.* **1980**, *63*, 228–229. doi:10.1111/j.1151-2916.1980.tb10700.x.
51. Mecif A, Soro J, Harabi A, Bonnet JP. Preparation of mullite- and zircon-based ceramics using kaolinite and zirconium oxide: A sintering study. *J. Am. Ceram. Soc.* **2010**, *93*, 1306–1312. doi:10.1111/j.1551-2916.2009.03595.x.
52. Kong Y, Yang Z, Zhang G, Yuan Q. Sliding friction and wear of alumina-reinforced zirconia-toughened mullite composites. *Wear* **2002**, *252*, 607–613. doi:10.1016/S0043-1648(02)00018-2.
53. Lee WE, Jayaseelan DD, Zhang S. Solid-liquid interactions: The key to microstructural evolution in ceramics. *J. Eur. Ceram. Soc.* **2008**, *28*, 1517–1525. doi:10.1016/j.jeurceramsoc.2007.12.010.
54. Lee WE, Souza GP, McConville CJ, Tarvornpanich T, Iqbal Y. Mullite formation in clays and clay-derived vitreous ceramics. *J. Eur. Ceram. Soc.* **2008**, *28*, 465–471. doi:10.1016/j.jeurceramsoc.2007.03.009.
55. Sainz MA, Serrano FJ, Amigo JM, Bastida J, Caballero A. XRD microstructural analysis of mullites obtained from kaolinite-alumina mixtures. *J. Eur. Ceram. Soc.* **2000**, *20*, 403–412. doi:10.1016/s0955-2219(99)00183-1.
56. Bradecki A, Jonas S. Investigation of high-temperature reactions within the $ZrSiO_4$-Al_2O_3 system. *Ceram. Int.* **2010**, *36*, 211–214. doi:10.1016/j.ceramint.2009.07.007.
57. Koyama T, Hayashi S, Yasumori A, Okada K, Schmucker M, Schneider H. Microstructure and Mechanical Properties of Mullite/Zirconia Composites Prepared from Alumina and Zircon under Various Firing Conditions. *J. Eur. Ceram. Soc.* **1996**, *16*, 231–237. doi:10.1016/0955-2219(95)00142-5.